Edge Effect Analysis and Edge Defect Detection of Titanium Alloy Based on Eddy Current Testing

Yuedong Xie [1,2], Jiyao Li [1], Yang Tao [3], Shupei Wang [4], Wuliang Yin [3] and Lijun Xu [1,2,*]

[1] School of Instrumentation and Optoelectronic Engineering, Beihang University, Beijing 100191, China; yuedongxie@buaa.edu.cn (Y.X.); xiaoheidouljy@buaa.edu.cn (J.L.)

[2] Beijing Advanced Innovation Center for Big Data-Based Precision Medicine, Beihang University, Beijing 100191, China

[3] School of Electrical and Electronic Engineering, University of Manchester, Manchester M13 9PL, UK; taoyang@tju.edu.cn (Y.T.); wuliang.yin@manchester.ac.uk (W.Y.)

[4] Manchester Advanced Intelligent Equipment Research and Innovation Centre Ltd. (MAIERIC Ltd.), Manchester M13 9PL, UK; shupei.wang@attach.net.cn

[*] Correspondence: lijunxu@buaa.edu.cn

Abstract: Titanium alloy is widely used in the area of aerospace and aviation due to its excellent properties. Eddy current testing (ECT) is among the most extensively used non-destructive techniques for titanium alloy material inspection. However, most previous research has focused on inspecting defects far from the edge of the material. It is a challenging task for edge crack detection because of edge effect. This study aims to investigate the influences of sensor parameters on edge effect and defect detection capability, and in the meantime, optimize sensor parameters to improve the capability of edge defect detection. The simulation method for edge effect evaluation is proposed including the 2^k factorial design used for factor screening, and the regression model is fitted and validated for sensor design and optimization for edge defect detection. A simulation scheme is designed to investigate the defect detection capability. An approach comprehensively analyzing the influence of coil parameters on edge effect and defect detection capability is applied to determine the optimal coil parameters for edge defect detection.

Keywords: eddy current testing; edge effect; titanium alloy; finite element analysis; factorial design

1. Introduction

In the aerospace industry, the demand for titanium has expanded dramatically due to its intrinsic features of light weight, excellent corrosion resistance, and high strength, etc. Titanium alloy is widely used for airframe and engine parts of aircrafts [1]. To ensure the safety operation of those key structures of aircrafts, the detection of titanium alloy structures becomes increasingly important in aircraft maintenance programs.

Nondestructive Testing (NDT) is a variety of methods involving the identification and characterization of damages or defect of materials without altering the original attributes or damaging the test object. NDT techniques possess wide applications in aerospace, military and defense, composite defects characterization, and pipe and tube inspection [2]. Commonly used NDT techniques include ultrasonic testing (UT), thermography, radiographic testing (RT), and eddy current testing (ECT).

Among all NDT techniques, eddy current testing has the benefit of cost effective and detection efficient, and is especially sensitive to surface and near-surface defects. Other advantages of ECT include easy-operation and environmental-friendly. The principle of eddy current detection is based on electromagnetic induction [3,4]. More specifically, a coil carrying an alternating current will produce

an electromagnetic field (EMF) according to Faraday's law. With a conductive material being placed in the proximity of this changing magnetic field, eddy currents will be then induced in the material. The induced eddy currents generate a secondary magnetic field which can be detected by the receiving coil. If flaws exist on the surface or near the surface of the material, the presence of the flaw will disturb eddy current distribution, which in turn will cause impedance variation of the coil. The applied current passing through the coil is generally sinusoidal with a frequency ranging from hundred Hz to a few MHz [5]. To obtain the best response, the excitation frequency should be determined based on the test material and the depth of the defect.

Many works have been devoted to studying ECT [6–8], including electromagnetic (EM) computation, sensor design, optimization, and instrument development. The classic EM computation solution is proposed by Dodd and Deeds. By assuming the conductor is semi-infinite and axial symmetry (typically a coil placed above a plate or a coil encircling a tube), Dodd and Deeds proposed analytical solutions for eddy current phenomenon [9].

To our knowledge, only a few studies are devoted to investigating edge effect and edge defect detection. The edge effect in eddy current detection has been systematically investigated in [10]. An analytic 3D eddy current model was proposed and its edge effect was investigated in [11]. A truncated region eigen function expansion (TREE) model was built in [12–14] to investigate the edge defects. Many ways to detect edge defects were proposed in [15–19], such as dual-frequency eddy current and eddy current pulsed thermography. However, edge defect detection is very important to industrial safety. Defects commonly develop from the edge of the material because of stress concentrations [20]. Compared with non-edge defects, since the stress at edge defects is more concentrated, edge defects are easier to expand and bring higher security risks, and even cause accidents. However, it is challenging to identify and characterize edge defects due to edge effect, since both the defect and the edge of the material will distort eddy currents, leading to an overlapped response [21,22]. Therefore, it is urgent to quantitatively investigate edge effect and edge defect detection.

In this work, a method aiming to optimize coil parameters to improve the capability of edge defect detection is proposed. More specifically, this work investigates the influences of sensor parameters on edge effect and defect detection capability separately. Quantitative relationships between sensor parameters and edge effect, sensor parameters and defect detection capability were constructed. An approach making use of desirability functions to optimize multiple responses was applied in order to find a set of coil parameters that optimizes the capability of edge defect detection.

The quantitative relationship between sensor parameters and edge effect is investigated via the finite element method (FEM) in Section 2. The defect detection capability evaluation and the result of optimization of coil parameters are introduced in Section 3, followed by the conclusion as shown in Section 4.

2. Edge Effect Evaluation

This section investigates the relationship between sensor parameters and edge effect in eddy current testing based on finite element method (FEM) and factorial design. A simulation method for edge effect evaluation, including edge effect indicator selection, factor screening, and model fitting, is proposed to quantitatively describe the relationship between sensor parameters and edge effect for eddy current testing.

2.1. Modeling Geometry

Three-dimensional (3D) finite element method (FEM) models with different sensor parameters were built with ANSYS Maxwell. The simulation model contains a test piece, an EM sensor, and a computation region. The test piece used is a cuboid plate with the material of titanium alloy. The EM sensor used is a cylindrical copper coil placed above the test piece, as shown in Figure 1. The modeling parameters are listed in Table 1.
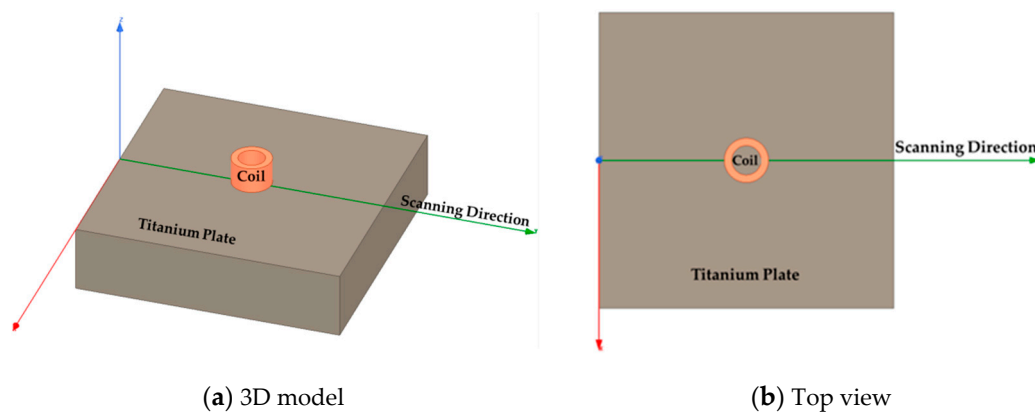
(**a**) 3D model   (**b**) Top view

Figure 1. Geometry of the simulation model.

Table 1. Material properties of simulation model.

Object	Material	Relative Permeability	Bulk Conductivity (Siemens/m)
Test piece	Titanium	1.00018	1,820,000
Electromagnetic sensor (Coil)	Copper	0.999991	58,000,000
Computation region	Vacuum	1	0

To investigate the influence of edge effect, parametric sweep was carried out with the coil perpendicularly scanned towards to the edge of the test piece, as shown in Figure 1. More specifically, the original position of the coil located above the center of the plate, and gradually it scanned along the y-axis to a position far away from the plate, in which area its self-inductance was basically not affected by the plate. The whole scanning path was 15 mm with a step of 0.2 mm.

The finite element method (FEM) subdivided the large model to smaller elements, as shown in Figure 2; the mesh quality determined the accuracy of the computed results. However, the very fine mesh/high mesh density was limited by the capacity of the computer and required more running times. The mesh operation should be modified to reach a balance between accuracy and the computing resource usage. The computation of the FEM solver is based on minimizing the energy error; in Figure 3, when the elements number is beyond 300,000, the energy error is as low as 0.005%, which is sufficiently accurate for the FEM computation. In this work, the mesh number used was around 370,000.
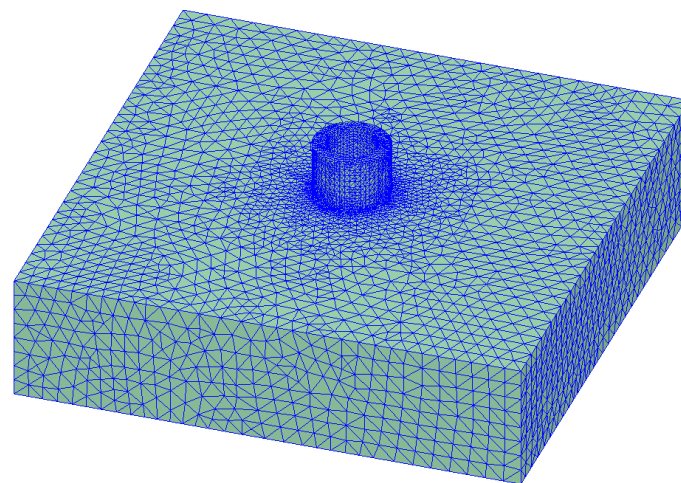

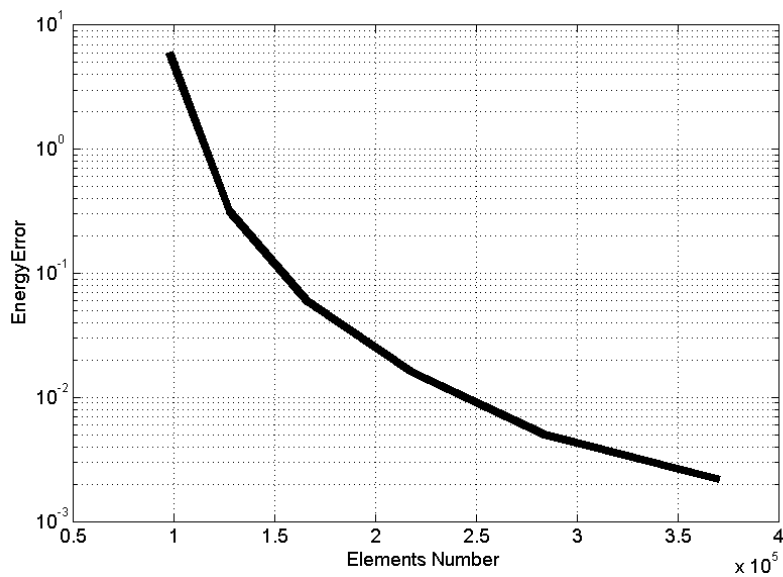**Figure 2.** Mesh plots of the simulation model.

Figure 3. Mesh-energy error curve.

2.2. Indicator Selection for Edge Effect Evaluation

In this paper, one single coil was used acting as transmitter and receiver simultaneously. The impedance of the coil was calculated based on Equation (1).

$$Z_n = \sqrt{(R - R_0)^2 + \omega^2 (L - L_0)^2} \tag{1}$$

where ω is the excitation frequency, ωL is the imaginary part of the complex impedance, and R is the real part of the complex impedance. R_0 and L_0 is the resistance and inductance of the coil when it is far from the test piece (air field).

Based on the modeling setup presented in Section 2.1, the self-inductance of the EM sensor varied along the scanning path as shown in Figure 4.
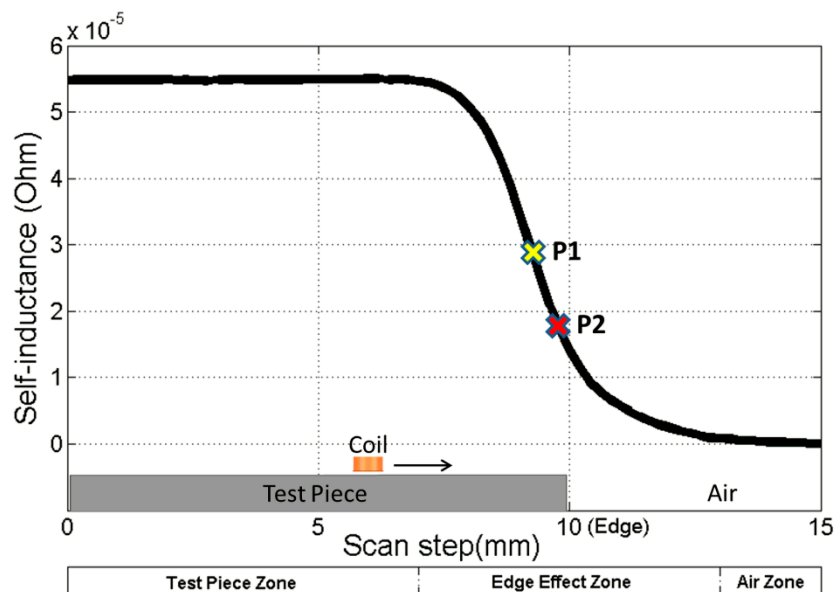

Figure 4. The self-inductance of the coil along the scanning path.

The coil located exactly above the edge of the test piece at the distance of 10 mm as shown in the "edge effect zone" in Figure 4. As shown in Figure 4, when the coil was scanned to a position away from the plate, its self-inductance was basically unchanged, which was recorded as L_1 (as shown in "air zone" in Figure 4). When the coil was scanned above the plate and was away from the edge, its self-inductance was also almost constant, which was recorded as L_2 (as shown in "test piece zone" in Figure 4). Between "test piece zone" and "air zone", the self-inductance of the EM sensor varied dramatically since the eddy current flow was distorted at the edge of the test piece.

Two indicators, D_{half} and $D_{30\%}$, were selected to quantitatively evaluate the edge effect. L_{half} means the half amplitude of the self-inductance as marked "P1" in Figure 4:

$$L_{half} = (L_1 + L_2)/2 \tag{2}$$

The distance between P1 and the edge (D_{half}) reveals the intensity of edge effect.

Similarly, 30% height point P2 can be defined, whose self-inductance is:

$$L_{30\%} = L_2 + 0.3 * (L_1 - L_2) \tag{3}$$

Additionally, define $D_{30\%}$ as the distance between P2 and the edge. Compared with D_{half}, $D_{30\%}$ is larger, so $D_{30\%}$ suffers less by scanning step size. To describe the edge effect comprehensively, both D_{half} and $D_{30\%}$ were taken as the edge effect indicators.

2.3. Factor Screening

For the model with a coil placed above a plate [6], the normalized coil impedance can be obtained by Equation (4).

$$Z = \frac{\pi\omega\mu n^2}{(l_2 - l_1)^2 (r_2 - r_1)} \int_0^\infty \frac{1}{\alpha^5} I^2(r_2, r_1) \Big((l_2 - l_1) + \alpha^{-1}\big\{ e^{-\alpha(l_2 - l_1)} - 1 \big\} \Big) \mathrm{d}\alpha \tag{4}$$

where l_1 and l_2 are the distance between the coil and the lower and upper surfaces of the metal plate. r_1 and r_2 are the inner and outer diameter of the coil. The coefficient α is determined by angular frequency ω, permeability μ, dielectric constant ε, and conductivity σ.

In order to investigate the edge effect, a variety of EM sensor parameters were investigated. According to Equation (4), five parameters of the EM sensor were selected as factors, including the ratio between the inner diameter and the outer diameter of the coil (denoted by "*A*"), coil height (denoted by "*B*"), lift-off ("*C*"), excitation frequency ("*D*"), and outer diameter ("*E*"). Based on the effect sparsity principle [23], only a few of the large group of factors were active, which means only some of the coil parameters affected the edge effect significantly. It is of necessity to perform factor screening experiments to determine the set of active parameters from the factors above.

A full factorial design was used for factor screening. Factorial designs have several important advantages over traditional one-factor-at-a-time experiments, including a reduced number of experiments, and possibilities to evaluate interactions among factors [24].

Because of the high computing resource usage of simulation, the number of simulations is limited; so the single replicate of 2^5 factorial design was used. The values that correspond to the high (+) and low (−) levels and the central point (0) for each factor are listed in Table 2.

Table 2. Values for each factor in 2^5 factorial design.

Symbols	Factors	Low(−)	High(+)	Central Point(0)
A	ratio between inner and outer diameter	0.5	0.65	0.575
B	height	1 mm	2 mm	1.5 mm
C	lift-off	0.1 mm	0.5 mm	0.3 mm
D	excitation frequency	50 kHz	100 kHz	75 kHz
E	outer diameter	1 mm	5 mm	3 mm

One approach to analyze the single replicate factorial design is to firstly examine the half-normal probability plot of the estimates of the effects [25]. Insignificant effects are normally distributed, with a mean of zero and tend to fall along the blue straight line as shown in Figure 5, whereas significant effects have nonzero means and hence do not lie along the straight line.
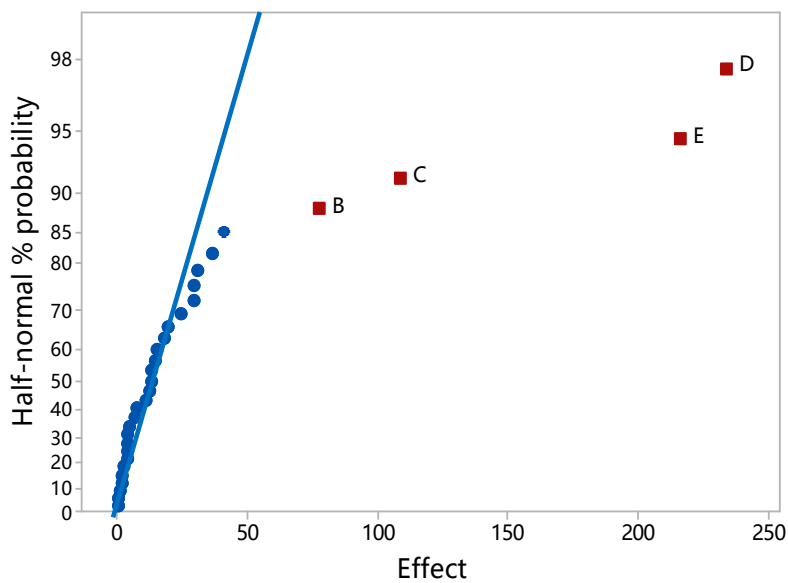
Figure 5. Half-normal probability plot of the effects for the 2^5 factorial ($D_{30\%}$).

The half-normal probability plot for $D_{30\%}$ and D_{half} is shown in Figures 5 and 6. All of the effects that lie along the blue line are negligible, whereas the large effects are far from the line. It can be seen that for $D_{30\%}$, the significant effects that emerge from this analysis are the main effects of "B" (coil height), "C" (lift-off), "D" (excitation frequency), and "E" (outer diameter), while for D_{half}, the significant effects comprise the main effects of "B", "C", "D" and "E", and "CE" interactions.

For either $D_{30\%}$ or D_{half}, "A" (ratio between inner and outer diameter) and all interactions involving "A" did not have a significant effect on edge effect, which means that factor "A" could be discarded from the simulation so that the experiment became a 2^4 factorial design with two replicates.

The ANOVA could then be used to determine which effects are significant to edge effect in a quantitative way. On the basis of the F-test, the effect is statistically significant if its p-value in the ANOVA output is less than a significant level. Usually the significant level is 0.05. The ANOVA is summarized in Tables 3 and 4; it can be concluded that main effects "B", "C", "D", and "E" significantly affected $D_{30\%}$. "B", "C", "D", "E", and interaction "CE" significantly influenced D_{half}.
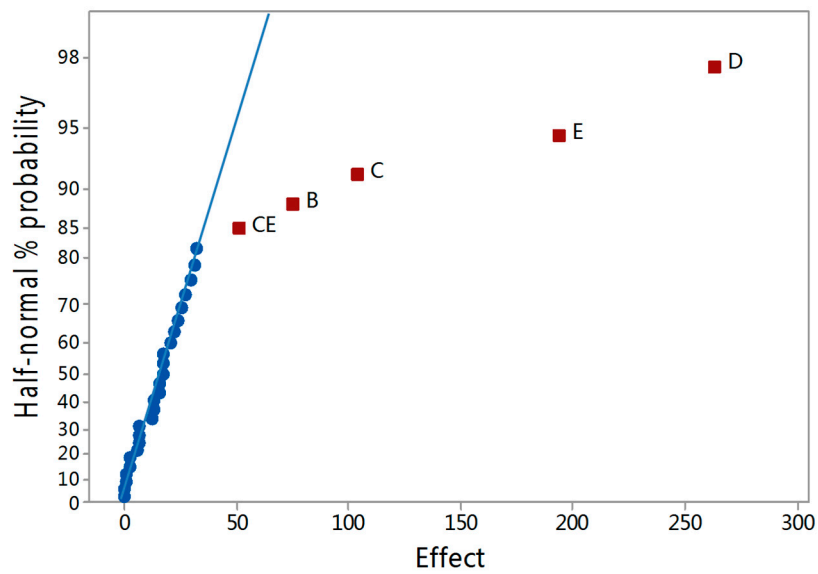
Figure 6. Half-normal probability plot of the effects for the 2^5 factorial (D_{half}).

Table 3. Analysis of Variance for $D_{30\%}$ in "B", "C", "D", and "E".

Source of Variation	Degree of Freedom	Sum of Squares	Mean Square	F_0	*p*-Value
Model	15	3.32697	0.2218	20.66	0
Linear	4	3.26675	0.81669	76.06	0
B	1	0.16503	0.16503	15.37	0.001
C	1	0.32413	0.32413	30.19	0
D	1	1.4968	1.4968	139.41	0
E	1	1.2808	1.2808	119.29	0
BC	1	0.00171	0.00171	0.16	0.695
BD	1	0.00058	0.00058	0.05	0.819
BE	1	0.00907	0.00907	0.84	0.372
CD	1	0.00006	0.00006	0.01	0.942
CE	1	0.04757	0.04757	4.43	0.051
DE	1	0.0001	0.0001	0.01	0.926
BCD	1	0.00009	0.00009	0.01	0.927
BCE	1	0.00055	0.00055	0.05	0.824
BDE	1	0.00045	0.00045	0.04	0.84
CDE	1	0.00001	0.00001	0	0.98
BCDE	1	0.00003	0.00003	0	0.962
Error	16	0.17179	0.01074		
Total	31	3.49876			

2.4. Model Fitting and Verification

After factor screening, effects which were significant to edge effect were obtained, and could be used to preliminary construct the first-order regression model. For D_{half}, it can be written as:

$$D_{half} = \beta_0 + \beta_1 * B + \beta_2 * C + \beta_3 * D + \beta_4 * E + \beta_{24} * CE \tag{5}$$

For $D_{30\%}$, it can be written as:

$$D_{30\%} = \gamma_0 + \gamma_1 * B + \gamma_2 * C + \gamma_3 * D + \gamma_4 * E \tag{6}$$

where "*B*", "*C*", "*D*", and "*E*" represent the linear effects of factors in Table 2. The term "*CE*" is the interaction of the linear lift-off with outside diameter. Other effects which were not significant were removed from the first-order model. $\beta_0, \beta_1, \ldots, \gamma_0, \ldots, \gamma_4$ are model coefficients.

Table 4. Analysis of Variance for D_{half} in B, C, D, and E.

Source of Variation	Degree of Freedom	Sum of Squares	Mean Square	F_0	*p*-Value
Model	15	2.09262	0.13951	27	0
Linear	4	2.00297	0.50074	96.93	0
B	1	0.09177	0.09177	17.76	0.001
C	1	0.17522	0.17522	33.92	0
D	1	1.12384	1.12384	217.54	0
E	1	0.61214	0.61214	118.49	0
BC	1	0.01243	0.01243	2.41	0.14
BD	1	0.00409	0.00409	0.79	0.387
BE	1	0.01457	0.01457	2.82	0.112
CD	1	0.00001	0.00001	0	0.964
CE	1	0.04245	0.04245	8.22	0.011
DE	1	0.00499	0.00499	0.97	0.34
BCD	1	0.00001	0.00001	0	0.973
BCE	1	0.01045	0.01045	2.02	0.174
BDE	1	0.00065	0.00065	0.13	0.728
CDE	1	0	0	0	0.986
BCDE	1	0	0	0	0.992
Error	16	0.08266	0.00517		
Total	31	2.17528			

All the experimental data were from previous factorial design, and the Least-square method was used to obtain model coefficient estimates. Suppose that n observations on the response are available. The response D_{halfi} and variables B_i, C_i, D_i, E_i, and CE_i denote the ith observation of the response and regressor variables. The model Equation (5) can be written in terms of observations as

$$D_{halfi} = \beta_0 + \beta_1 * B_i + \beta_2 * C_i + \beta_3 * D_i + \beta_4 * E_i + \beta_{24} * CE_i + \varepsilon_i \tag{7}$$

where ε_i is the error term. The least square function is

$$L = \sum_{i=1}^{n} \varepsilon_i^2 \tag{8}$$

The method of least squares chooses the βs in Equation (7) so that the sum of the squares of the errors L is minimized.

The fitted model of response D_{half} using Least-square method is

$$D_{half} = 1.0286 + 0.06036B + 0.3318C - 0.003206D + 0.1768E - 0.03805CE \tag{9}$$

The fitted model of response $D_{30\%}$ can be obtained using the same method

$$D_{30\%} = 1.8535 + 0.1160B + 0.3625C - 0.008577D + 0.11883E \tag{10}$$

The result of testing for lack of fit shown in Table 5 indicates that there was no strong evidence of lack of fit, so there was no need to construct a higher order regression model.

To validate the predicting ability of this regression model, five additional simulations were conducted. The coil parameters used in these five experiments were out of range of the original parameters in factorial design. It turned out that all these five observations fell inside the prediction interval on the response at that point, which provided some assurance that the regression models can

describe the quantitative relationship between coil parameters and the edge effect. Such results can be applied to sensor design and optimization especially for edge defect detection.

Table 5. Lack-of-fit tests.

Response	Mean Square	F_0	*p*-Value
D_{half}	0.000140	0.34	0.998
$D_{30\%}$	0.000540	0.49	0.969

3. The Defect Detection Capability Evaluation

This section aims to investigate the detection capability of different combinations of sensor parameters using the finite element method (FEM). Two indications were selected as the responses representing the detection capability. The methodology used to construct the quantitative relationship is similar to that in Section 2.

3.1. Simulation Model

The only difference in the simulation model was that a defect was added to the plate. As shown in Figure 7, the scanning path is along the *Y* axis, perpendicular to the edge and the long side of the defect. The parameters of the defect are shown in Table 6.

(**a**) 3D model   (**b**) Top-view
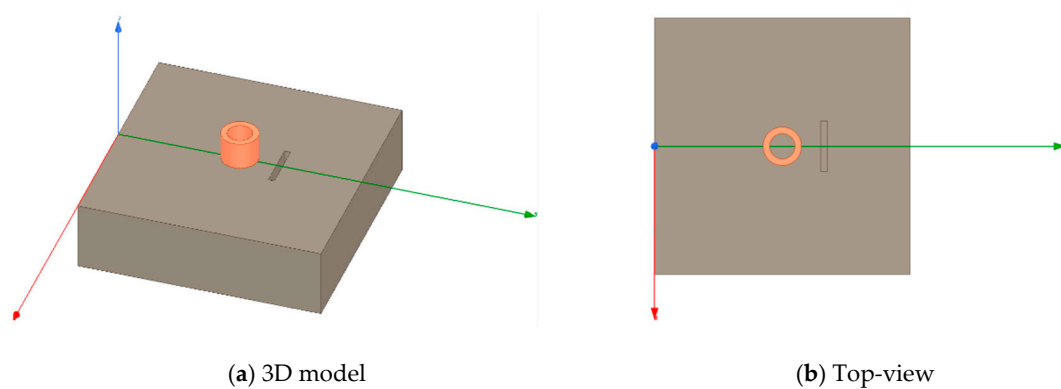
Figure 7. Geometry of the simulation model.

Table 6. Defect information.

Shape	Length (mm)	Depth (mm)	Width (mm)	Distance from the Right Edge (mm)
cuboid	4	2	0.5	7

The whole length of the scanning path was 15 mm. The coil firstly reached the defect, at 7 mm, which caused a small dip in the self-inductance curve (Figure 8). Then, it reached the edge at 10 mm. At the end of the scanning path, the coil was away from the plate, so its self-inductance reached a relatively steady state.

Two indicators were defined from Figure 8 to represent the detection capability of the coil:

1. The Distance between Dip Position and the Real Position of edge (*DIS*)

Dis reflects the possibility of defect detection affected by edge effect. The higher the *DIS* is, the lower the possibility that dip signal caused by defect will overlap with edge signal, and the easier the edge defect being detected.

2. Dip–Dip Ratio (*RATIO*)

Firstly, define two variables L_{p-v} and L_{h-v}, as marked in Figure 8. *RATIO* is the ratio between L_{p-v} and L_{h-v}. If *RATIO* is large enough, the defect can be easily recognized even when the dip signal caused by defect overlaps with edge signal.
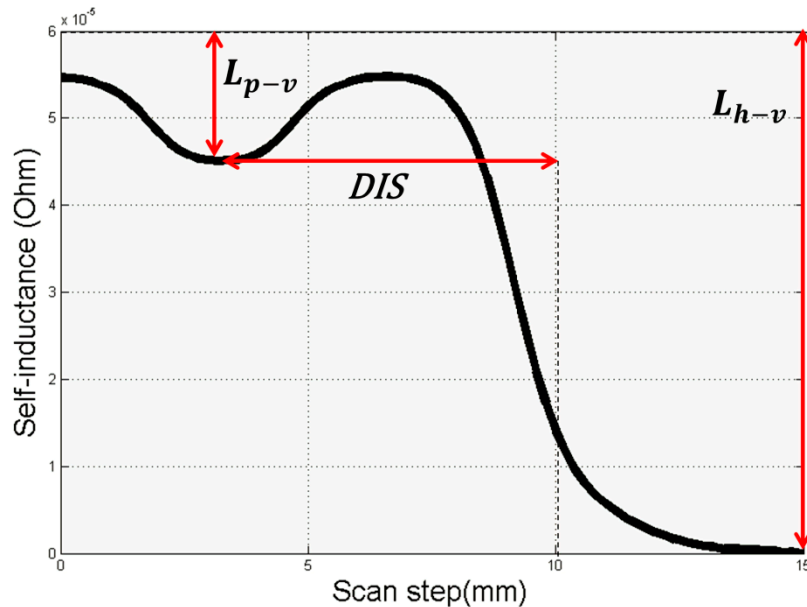

Figure 8. Self-inductance curve (with defect).

3.2. Simulation Scheme

The result of factor screening in Section 2 showed that the ratio of inner and outside diameter did not have significant effect on edge effect, so it was discarded from the regression models constructed in Section 2. In order to facilitate the latter analysis, 4 factors out of 5 mentioned in Section 2 were investigated to construct regression model as shown in Table 7. The values that correspond to the high(+) and low(−) levels and the central point(0) for each factor are the following:

Table 7. Values for each factor in 2^5 factorial design.

Symbols	Factors	Low(−)	High(+)	Central Point(0)
A	height	1 mm	2 mm	1.5 mm
B	lift-off	0.1 mm	0.5 mm	0.3 mm
C	outside diameter	1 mm	5 mm	3 mm
D	excitation frequency	50 kHz	100 kHz	75 kHz

3.2.1. First-Order Model Design

The first step was to preliminarily fit the first-order model. A 2^4 full factorial design with three replicates of the central point was used. After discarding the effects which were insignificant and obtaining model coefficient estimates by the Least-square method, the following models were obtained:

$$DIS = 6.12 + 0.63A + 0.78B + 0.20C - 1.34AB - 0.21AC - 0.021BC + 0.40ABC \tag{11}$$

$$RATIO = 1.21 - 0.36A - 1.61B - 0.30C - 0.0046D + 0.58AB + 0.10AC + 0.47BC + 0.19ABC \tag{12}$$

where the symbols *A*, *B*, *C*, *D*, and their corresponding factors are listed in Table 7.

Table 8 shows lack-of-fit statistics of the first-order regression models above. It can be seen that Model (9) had insignificant lack-of-fit, while it was reasonable to add quadratic terms in the regression model involving *RATIO* and coil parameters.

Table 8. Lack-of-fit tests (first-order model).

Response	Mean Square	F_0	*p*-Value
DIS	0.000411	0.1	0.999
RATIO	0.000078	0.67	0.802

3.2.2. Second-Order Model Design

The face-centered central composite design (FCCCD) was used for fitting a second-order model involving *RATIO* and coil parameters. FCCCD is a variation of the central composite design (CCD), and is a popular class of designs for fitting second-order models. It consists of a 2^k factorial design, 2k axial runs, and multiple center runs. Its advantage over CCD is that it only requires 3 levels of each factor, so that the actual values of coil parameters will not go beyond the set range before.

The following model was obtained:

$$RATIO = 0.696 - 0.26A - 0.66B - 0.13C + 0.00076D + 0.026A^2 + 0.23AB + 0.036\,AC + 0.15BC - 0.065ABC \quad (13)$$

Table 9 shows lack-of-fit statistics of Model (13). The result of testing for lack of fit showed that there was no strong evidence of lack of fit. So, Model (13) is better than Model (12) in describing the quantitative relationship between *RATIO* and coil parameters. It can be seen that in Models (12) and (13), the effect of excitation frequency was the opposite. The main reason is that Model (12) has nonnegligible lack-of-fit, so error exists in coefficient estimation, especially for factors such as frequency, which has a weak influence on the response. By comparison, Model (13) provides a more accurate estimation: as the excitation frequency grows, the *RATIO* increases, and the detection capability improves.

Table 9. Lack-of-fit tests (second-order model).

Response	Mean Square	F_0	*p*-Value
RATIO	0.000051	0.43	0.954

The predicting ability of this regression model was validated using the same method mentioned in Section 2.4. The result was satisfactory.

Based on the analysis above, Models (11) and (13) can be used to evaluate the quantitative relationship between detection capabilities and coil parameters.

3.2.3. Influence of Defect Location and Width

In order to investigate the influence of the location and dimensions of defect on *DIS* and *RATIO*, two control experiments were conducted. The defect information of control group is the same as that in Table 6, and the information of experimental groups is shown in Table 10.

Table 10. Defect information of experimental groups.

Group	Length (mm)	Depth (mm)	Width (mm)	Distance from the Right Edge (mm)
Control	4	2	0.5	7
Experimental 1	4	2	0.5	5
Experimental 2	4	2	1	7

The defect in Experimental Groups 1 was 2 mm closer to the edge than the control group, and the difference between Experimental Group 2 and the control group was the width of the defect.

For ease of comparison, Experimental Groups 1 and 2 were also conducted using 2^4 full factorial design. The means of DIS and RATIO were compared to evaluate the differences between the control group and the experimental groups.

1. *DIS*

The comparation results is shown in Table 11:

Table 11. Comparison results of *DIS*.

Group	Mean	Standard Deviation	Mean Standard Error
Control	3.2474	0.1073	0.0246
Experimental 1	5.2368	0.1116	0.0256

The mean difference between the two groups was 1.9894 mm, very close to 2 mm, which means that with the change of defect position, the position of defect wave peak will move the same distance in the same direction. Therefore, the regression model of dip position obtained by the control group only needs to change the constant term, which can be directly used for defects with the same shape and size but in different positions.

2. *RATIO*

The comparation results is shown in Table 12.

Table 12. Comparison results of *RATIO*.

Group	Mean	Standard Deviation	Mean Standard Error
Control	0.2525	0.0866	0.0199
Experimental 1	0.2544	0.0793	0.0182
Experimental 2	0.3099	0.1174	0.0391

The mean difference between the control group and the experimental group 1 was relatively small; however, the mean value of *RATIO* in experimental group 2 was much larger than that in the control group. So, it can be assumed that the location of the defect has no influence on *RATIO*, while as the width of the defect increases, the value of *RATIO* also increases significantly.

3.3. Optimization of Coil Parameters

During the analysis above, three distance responses were defined: $D_{half}, D_{30\%}$ and *DIS*. D_{half} and $D_{30\%}$ represent the scope of influence of edge effect, while DIS represents the distance between the edge and dip caused by the defect. The smaller D_{half} and $D_{30\%}$ and the larger *DIS*, the lower the possibility of the dip caused by defect mixing with edge effect, so a new response was defined with a combination of the three responses above:

$$SPA = DIS - \frac{\left(D_{half} + D_{30\%}\right)}{2} \tag{14}$$

For defect detection, especially edge defect detection, it would be desirable if *SPA* and *RATIO* became larger simultaneously so that the dip caused by edge defect could be easily identified.

In order to find a set of coil parameters that optimizes the capability of edge defect detecting, an approach making use of desirability functions to optimize multiple responses was applied [26]. The approach converted responses *SPA* and *RATIO* into their individual desirability functions d_1 and d_2 that vary from 0 to 1:

$$d_i \ (i = 1,\ 2) = \begin{cases} 0 & y < L_i \\ \frac{y_i - L_i}{T_i - L_i} & L_i \leq y \leq T_i \\ 1 & y > T_i \end{cases} \tag{15}$$

where y_i is the value of the response. L_i and T_i are the lower and upper limits of the response, respectively, and were set to the maximum and minimum values of the response in previous simulation,

shown in Table 5. If the value of response comes closer to its target T_i, then d_i comes closer to 1. The coil parameters' upper and lower limits during optimization are also shown in Table 13.

Table 13. Settings for optimization.

Name	Lower Limit	Upper Limit	Unit
Coil height	1	2	mm
Lift-off	0.1	0.5	mm
Excitation frequency	50	100	kHz
Outer diameter	1	5	mm
SPA	4.51	5.89	mm
RATIO	0.12	0.41	none

The coil parameters were then chosen to maximize the overall desirability

$$D = (d_1 * d_2)^{1/2} \tag{16}$$

Table 14 shows the top 5 solutions with the highest overall desirability. It can be seen that under the constraints of each parameter, an EM coil with a height of 1 mm, an outer diameter of 1 mm, and excitation frequency of 100 kHz lifted 0.1 mm off the test piece was the best one in detecting edge defect.

Table 14. Solutions with the highest overall desirability.

Number	Height	Lift-off	Frequency	Diameter	*DIS*	*RATIO*	Desirability
1	1	0.1	100	1	5.72899	0.394245	0.92
2	1	0.1	99.77	1	5.7273	0.393994	0.919
3	1	0.1	98.81	1	5.72142	0.393337	0.916
4	1.03	0.1	100	1	5.73143	0.391007	0.915
5	1	0.1	99.99	1.03	5.72501	0.391539	0.914

It should be noted that in Section 3 only one specific kind of defect was studied, so theoretically all the regression models constructed in Section 3 are only available for the specific defect. However, it is reasonable that the best solution can be applied to all rectangular defects of similar size.

4. Conclusions

This study proposed a methodology to optimize coil parameters for edge defect detection. Two responses ($D_{half}, D_{30\%}$) were defined to describe edge effect and another two responses (*DIS* and *RATIO*) were defined to evaluate the defect detecting capability. Coil parameters which were truly significant to the responses were selected using screening experiments. Regression models were then obtained for $D_{half}, D_{30\%}$, *DIS* and *RATIO* responses. A new response *SPA* was defined with a combination of $D_{half}, D_{30\%}$, and *DIS*. It turned out that the larger the *SPA*, the lower the possibility that the dip caused by defect is affected by edge effect. The larger the *RATIO*, the easier the dip caused by defect is identified. An approach making use of desirability functions to both maximize *SPA* and *RATIO* was applied, and the best set of coil parameters in detecting edge defect was found. The proposed methodology can be extended to other sensor parameters and crack parameters analysis.

There is still some follow-up work to investigate in the future. Firstly, the scanning path parallel to the edge might be less sensitive to edge effect, so it might provide better results in detecting edge defect. Secondly, other kinds of sensor including a differential sensor or absolute sensor with a transmitter and a receiver will be investigated. Thirdly, deep learning will be used to estimate the location and size of edge defect. In addition, more simulations and experiments at a relatively higher excitation frequency such as 500 kHz, 1 MHz, and 2 MHz will be conducted to investigate the excitation frequency effect for edge defect detection, especially the small edge defect detection.

References

1. Inagaki, I.; Takechi, T.; Shirai, Y.; Ariyasu, N. Application and features of titanium for the aerospace industry. *Nippon Steel Sumitomo Met. Tech. Rep.* **2014**, *106*, 22–27.

2. Dwivedi, S.K.; Vishwakarma, M.; Soni, A. Advances and Researches on Non Destructive Testing: A Review. *Mater. Today Proc.* **2018**, *5*, 3690–3698. [CrossRef]

3. Sophian, A.; Tian, G.Y.; Taylor, D.; Rudlin, J. Electromagnetic and eddy current NDT: A review. *Insight Non-Destr. Test. Cond. Monit.* **2001**, *43*, 302–306.

4. Abdalla, A.N.; Faraj, M.A.; Samsuri, F.; Rifai, D.; Al-Douri, Y. Challenges in improving the performance of eddy current testing: Review. *Meas. Control Lond. Inst. Meas. Control* **2018**, *52*, 002029401880138. [CrossRef]

5. Bray, D.E. *Nondestructive Evaluation, a Tool in Design, Manufacturing and Service*; CRC: Boca Raton, FL, USA, 1997; pp. 51–58.

6. Abidin, I.Z.; Tian, G.Y.; Wilson, J.; Yang, S.; Almond, D. Quantitative evaluation of angular defects by pulsed eddy current thermography. *NDT E Int.* **2010**, *43*, 537–546. [CrossRef]

7. Munalli, D.; Dimitrakis, G.; Chronopoulos, D.; Greedy, S.; Long, A. Electromagnetic shielding effectiveness of carbon fibre reinforced composites. *Compos. Part B Eng.* **2019**, *173*, 106906. [CrossRef]

8. Li, X.; Gao, B.; Woo, W.L.; Tian, G.Y.; Qiu, X.; Gu, L. Quantitative surface crack evaluation based on eddy current pulsed thermography. *IEEE Sens. J.* **2016**, *17*, 412–421. [CrossRef]

9. Dodd, C.V.; Deeds, W.E. Analytical Solutions to Eddy-Current Probe-Coil Problems. *J. Appl. Phys.* **1968**, *39*, 2829–2838. [CrossRef]

10. Hagemaier, D.J. Eddy current impedance plane analysis. *Mater. Eval.* **1983**, *41*, 211–218.

11. Paul, S.; Bird, J.Z. Analytic 3-D eddy current model of a finite width conductive plate including edge-effects. *Int. J. Appl. Electromagn. Mech.* **2014**, *45*, 535–542. [CrossRef]

12. Theodoulidis, T.P.; Bowler, J.R. Eddy current coil interaction with a right-angled conductive wedge. *Proc. R. Soc. A Math. Phys. Eng. Sci.* **2005**, *461*, 3123–3139. [CrossRef]

13. Bowler, J.R.; Theodoulidis, T.P. Coil impedance variation due to induced current at the edge of a conductive plate. *J. Phys. D Appl. Phys.* **2006**, *39*, 2862. [CrossRef]

14. Theodoulidis, T.P.; Bowler, J.R. Interaction of an eddy-current coil with a right-angled conductive wedge. *IEEE Trans. Magn.* **2010**, *46*, 1034–1042. [CrossRef]

15. Sasi, B.; Rao, B.P.C.; Jayakumar, T. Dual-frequency eddy current non-destructive detection of fatigue cracks in compressor discs of aero engines. *Def. Sci. J.* **2004**, *54*, 563. [CrossRef]

16. Sharma, S.; Udpa, L.; Sun, Y.; Udpa, S. A modified differential pickup reflection probe. In *Review of Progress in Quantitative Nondestructive Evaluation*; Springer: Boston, MA, USA, 1998; pp. 1051–1058.

17. Zenzinger, G.; Bamberg, J.; Satzger, W.; Carl, V. Thermographic crack detection by eddy current excitation. *Nondestruct. Test. Eval.* **2007**, *22*, 101–111. [CrossRef]

18. He, C.; Tian, Y.P.; Wang, S.S.; Li, T.Y.; Zhou, K.Y. Simulation and Defect Identification of Eddy-Current Induced Thermography. In Proceedings of the 2014 Quantitative InfraRed Thermography, Bordeaux, France, 7–11 July 2014.

19. Zhu, J.; Jian-Bo, W.U.; Tian, G.Y.; Gao, Y.I. Detection and Reconstruction of Rolling Contact Fatigue Cracks Using Eddy Current Pulsed Thermography. In Proceedings of the 2018 IEEE Far East NDT New Technology & Application Forum, Xiamen, China, 6–8 July 2018.

20. Yang, S.; Tian, G.; Abidin, I.Z.; Wilson, J. Simulation of edge cracks using pulsed eddy current stimulated thermography. *J. Dyn. Syst.* **2011**, *133*, 011008. [CrossRef]

21. Alatawneh, N.; Underhill, P.R.; Krause, T.W. Low-frequency eddy-current testing for detection of subsurface cracks in cf-188 stub flange. *IEEE Sens. J.* **2018**, *18*, 1568–1575. [CrossRef]

22.   Wang, Y.B.; Bai, Q.; Du, W.; Zhang, B. Edge Effect on Eddy Current Detection for Subsurface Defects in Titanium Alloys. In Proceedings of the 8th International Conference on Computational Methods, Guilin, China, 25–29 July 2017.

23.   Montgomery, D.C. *Design and Analysis of Experiments*; Wiley: Hoboken, NJ, USA, 1976; pp. 179–307, 460–568.

24.   Tarley, C.R.T.; Silveira, G.; Santos, W.N.L.D.; Matos, G.D.; Silva, E.G.P.D.; Bezerra, M.A. Chemometric tools in electroanalytical chemistry: Methods for optimization based on factorial design and response surface methodology. *Microchem. J.* **2009**, *92*, 58–67. [CrossRef]

25.   Daniel, C. Use of half-normal plots in interpreting factorial two-level experiments. *Technometrics* **1959**, *1*, 311–341. [CrossRef]

26.   Derringer, G.; Suich, R. Simultaneous optimization of several response variables. *J. Qual. Technol.* **1980**, *12*, 214–219. [CrossRef]

Publisher's Note: MDPI stays neutral with regard to jurisdictional claims in published maps and institutional affiliations.